

Yield-Stress and Creep Control Depot Formation and Persistence of Injectable Hydrogels Following Subcutaneous Administration

Carolyn K. Jons, Abigail K. Grosskopf, Julie Baillet, Jerry Yan, John H. Klich, Olivia M. Saouaf, and Eric A. Appel*

Hydrogels that can be injected into the body using standard needles or catheters enable a minimally invasive strategy to prolong local delivery of therapeutic cargo. In particular, physically cross-linked hydrogels exhibit shear-thinning and self-healing behaviors enabling facile injectability and depot formation upon administration. While prior efforts to characterize these systems have focused on injectability and cargo release behaviors, prediction of cargo release in the body often assumes these materials form a depot rather than spreading out upon administration. Here, it is evaluated how hydrogel rheology correlates with depot formation and persistence following subcutaneous administration in mice with two physicochemically distinct, physically cross-linked hydrogel systems. Calcium-alginate and polymer-nanoparticle hydrogel systems exhibit variable mechanical behaviors across several rheological properties (stiffness, viscoelasticity, yield stress, and creep). By relating measured rheological properties to depot formation and persistence time following subcutaneous administration, it is identified that yield stress is predictive of initial depot formation while creep is predictive of depot persistence for these two gel systems. Indeed, only materials with yield stresses >25 Pa form robust depots, and reduced creep correlates with longer depot persistence. These findings provide predictive insights into design considerations for hydrogel technologies capable of extended controlled release of therapeutic cargo.

USD 2.2 trillion by 2026.^[1] Hydrogels are a particularly exciting controlled delivery platform that are characterized by cross-linked macromolecular networks retaining a significant amount of water and which have been utilized for a range of translational applications including immunology,^[2,3] oncology,^[4-6] cardiology,^[7-9] tissue engineering,^[10,11] wound healing,^[12-15] and pain management.^[16] Their high water content is advantageous as it provides physicochemical similarity to biological tissues and allows for the encapsulation of therapeutic cells and hydrophilic drug cargo, while the presence of a polymer network imparts physical structure, tunable mechanical properties, and controlled cargo diffusion or cell motility.^[17-19]

Hydrogels allow for control over how drugs are available to cells and tissues over time and in space. Greater control over spatial and temporal drug delivery allows for improved therapeutic outcomes by enhancing treatment efficacy while reducing toxicity and required dosage.^[20-22]

Hydrogels that can be injected into the body using standard needles or catheters enable a minimally invasive strategy to prolong local delivery of therapeutic cargo, whether cells or pharmaceuticals. In particular, physically cross-linked hydrogels

1. Introduction

Drug delivery is a pressing problem with the global controlled pharmaceutical delivery market projected to exceed

C. K. Jons, J. Baillet, O. M. Saouaf, E. A. Appel
Department of Materials Science & Engineering
Stanford University
Stanford, CA 94305, USA
E-mail: eappel@stanford.edu

A. K. Grosskopf
Department of Chemical Engineering
Stanford University
Stanford, CA 94305, USA


J. Baillet
CNRS, Bordeaux INP, LCPO
University of Bordeaux
Pessac 33600, France

J. Yan, J. H. Klich, E. A. Appel
Department of Bioengineering
Stanford University
Stanford, CA 94305, USA

E. A. Appel
Stanford ChEM-H Institute
Stanford University
Stanford, CA 94305, USA

E. A. Appel
Woods Institute for the Environment
Stanford University
Stanford, CA 94305, USA

E. A. Appel
Department of Pediatrics Endocrinology
Stanford University School of Medicine
Stanford, CA 94305, USA

 The ORCID identification number(s) for the author(s) of this article can be found under <https://doi.org/10.1002/adfm.202203402>.

DOI: 10.1002/adfm.202203402

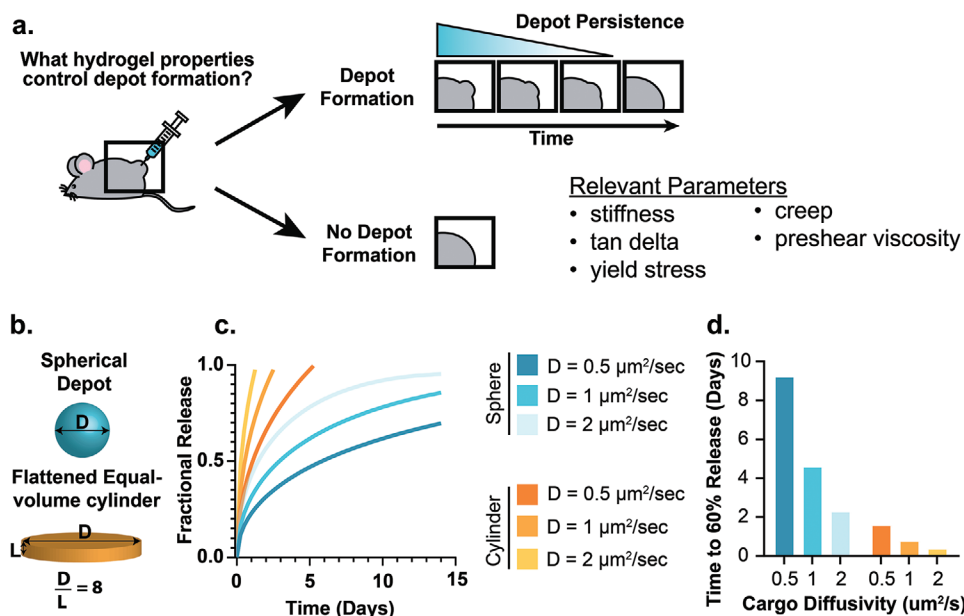


Figure 1. Schematic of injectable hydrogel depot formation and persistence. a). Illustration of depot persistence as compared to rapid flattening following subcutaneous administration. b). Illustration of spherical and cylindrical hydrogel depots. c). Cargo release profiles from spherical and cylindrical depots with varied diffusion coefficients as predicted by the Ritger–Peppas model. d). Impact of depot geometry and diffusion coefficient on time to 60% release of the entrapped cargo.

exhibit shear-thinning and self-healing behaviors enabling facile injectability and self-healing upon administration.^[23–26] Subcutaneous administration is often a preferred means of drug administration as it is even sufficiently simple to allow for facile self-administration by patients.

The modeling of release kinetics from a polymeric drug delivery system in the body is often simplified by assuming the formation of a spherical depot following subcutaneous administration.^[27,28] Yet, after administration, the material may deform or flatten under the stresses present in the subcutaneous space (Figure 1a).^[29,30] This shape change has significant impact on diffusion length and corresponding release kinetics. The most common kinetic model used in drug release studies is the Ritger–Peppas model,^[31] which describes drug transport through both Fickian diffusion and anomalous transport mechanisms. Comparing Fickian release behaviors alone from an equal-volume sphere and cylinder (aspect ratio eight) (Figure 1b) demonstrates depot shape heavily impacts cargo release kinetics (Figure 1c), and that a spherical depot will result in a four-fold greater time to 60% release of the entrapped cargo (Figure 1d). Additionally, a flattened cylinder has an increased surface area to volume ratio that would likely further increase the rate of erosion and correspondingly shortens drug release timescales. Although simple modeling shows that shape heavily impacts drug release kinetics from polymeric drug delivery systems, little effort has focused on understanding and predicting spherical depot formation following hydrogel administration in the body. In this work, we seek to address this crucial gap in knowledge to elucidate how rheological properties of hydrogels are relevant to maintaining depot shape and persistence in the body.

To probe the impact of gel rheological properties on depot formation and persistence, we first sought to evaluate the properties of a range of physically cross-linked hydrogel

systems from two physiochemically distinct chemistries for two crucial reasons: i) to identify of a subset of hydrogel compositions that span a range of rheological properties, and ii) and to obtain specific rheological property values that could be directly related to depot formation and persistence in vivo. To achieve these goals, we evaluated both calcium-alginate and polymer-nanoparticle (PNP) hydrogel formulations (Figure 2). PNP hydrogels are self-assembled from dynamic, multivalent, and entropically driven non-covalent interactions between nanoparticles and high-molecular-weight biopolymers (Figure 2a).^[32] We have previously reported PNP hydrogels formulated with poly(ethylene glycol)-b-poly(lactic acid) nanoparticles (PEG-PLA NPs) and dodecyl-modified hydroxypropyl methylcellulose polymers (HPMC-C₁₂),^[33] whereby the HPMC-C₁₂ polymers form a dynamic corona that surrounds and bridges between nanoparticles upon mixing of the two components.^[34] These materials are shear thinning and injectable and have been successfully utilized for various biomedical applications including prolonged delivery of therapeutic molecules and cells, post-operative adhesion barriers, stabilization of biopharmaceuticals, and prolonged delivery of wildland fire retardants for wildfire prevention.^[8,35–38] Calcium-alginate hydrogels, on the other hand, are formed through the cross-linking of sodium alginate by calcium ions (Figure 2d). The cross-linking occurs through exchange of sodium ions from guluronic acid residues that make up segments of the polysaccharides with multivalent cations such as calcium or barium in aqueous media.^[39] On account of their simple and mild cross-linking chemistry, calcium-alginate hydrogels have been used in a multitude of therapeutic molecule and cell delivery, wound dressing, tissue engineering, and bioprinting applications.^[40–44]

An array of both calcium-alginate and PNP hydrogel formulations can be easily generated to access materials exhibiting a

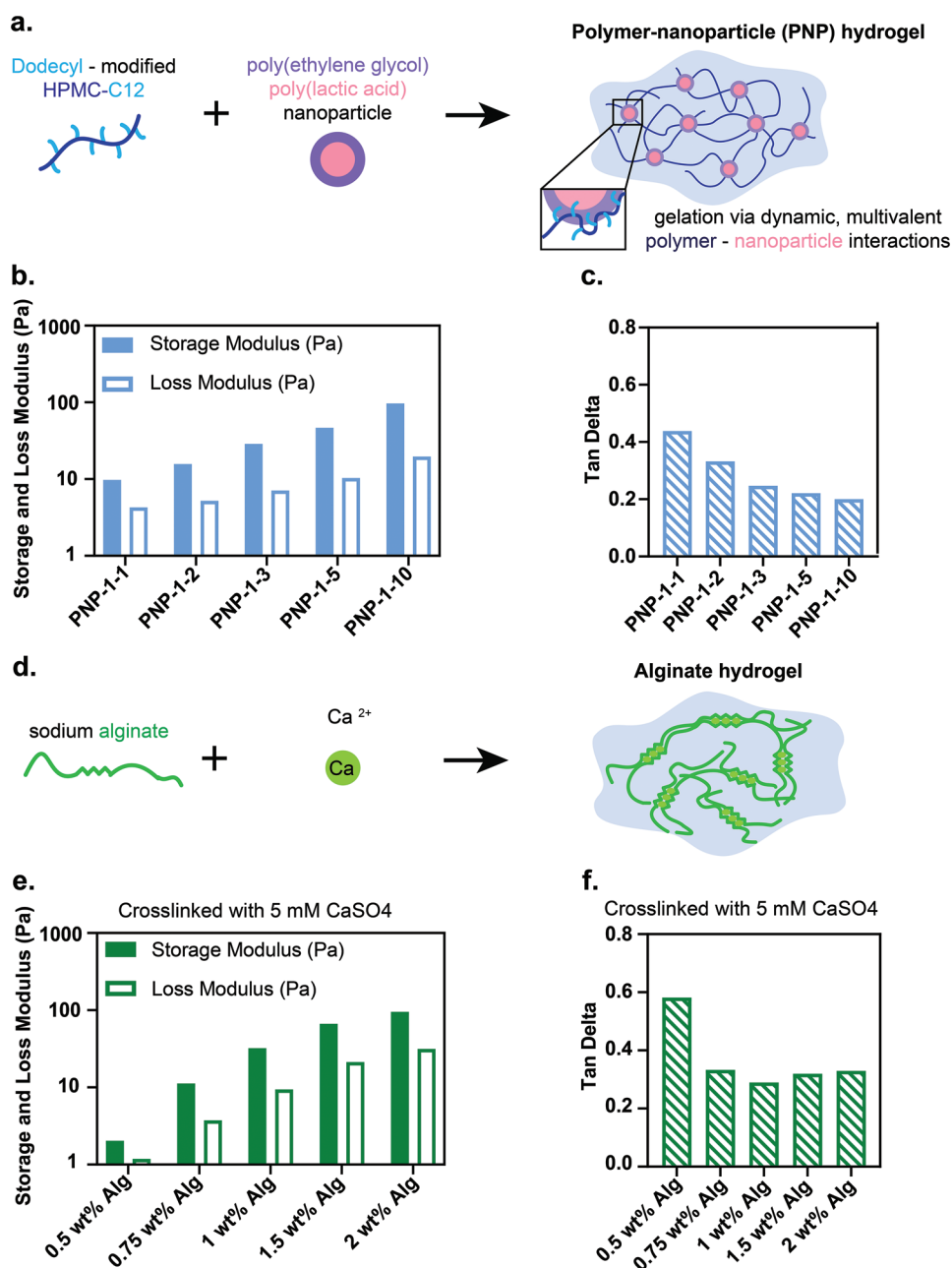


Figure 2. Two distinct non-covalently cross-linked hydrogels have tunable rheological properties. a). Formulation of polymer-nanoparticle hydrogel. b). Storage and loss moduli of PNP hydrogel formulations. c). Tan delta of PNP hydrogel formulations. d). Formulation of alginate hydrogel. e). Storage and loss moduli of alginate hydrogel formulations. f). Tan delta of alginate hydrogel formulations.

broad range of rheological properties. We have reported previously that the stiffness, viscosity, and relative elasticity of PNP hydrogels is increased by increasing nanoparticle concentration and tuning the P-NP ratio.^[8,36,45] Prior work in the field has additionally informed how changing the composition of calcium-alginate hydrogels results in control over rheological properties. By increasing either polymer composition^[46] or calcium content,^[47] calcium-alginate hydrogels increase in stiffness and viscosity. Additionally, alginate molecular weight is predictive of stress-relaxation and creep behavior in these materials.^[48] While prior work has investigated the rheological behavior of calcium-alginate

and PNP gel systems, individual studies rarely fully characterize the stiffness, viscosity, yielding, and creep behavior of a given hydrogel formulation. In this work, we show that either increasing the concentration of alginate at a constant calcium content^[46] or increasing the concentration of PEG-PLA NPs at a constant HPMC-C₁₂ concentration^[45] yields hydrogels with more solid-like properties, higher yield stresses, higher preshear viscosities, and decreased creep behavior (Figure 2b,e). By formulating both PNP and calcium-alginate hydrogels with a spectrum of rheological properties, thoroughly characterizing the mechanical properties of these materials, and monitoring their behavior

upon subcutaneous administration in mice, we aim to elucidate relationships between rheological behaviors and the ability to form and maintain depots following injection that can yield generalizable design criteria for injectable hydrogels.

2. Results and Discussion

2.1. Rheological Characterization of PNP and Alginate Hydrogels

To capture a range in gel rheological properties, we created five PNP hydrogels with a uniform HPMC-C₁₂ polymer content of 1 wt.% and varied PEG-PLA NP contents of 1, 2, 3, 5, and

10 wt.%. PNP hydrogel formulations are referred to in the format P-NP, whereby P denotes the weight percent of HPMC-C₁₂ and NP denotes the weight percent of the PEG-PLA NPs. The remaining mass of the formulation is phosphate-buffered saline. As the PEG-PLA NPs act as cross-linkers in the PNP hydrogel system, increasing NP content in these materials results in hydrogels with more solid-like properties as indicated by the increase in storage modulus and decrease in tan-delta (Figure 2b,c), (Figures S1 and S2, Supporting Information). Furthermore, NP content impacted both yield stress and preshear viscosity. Stress-controlled yield stress measurements evaluate hydrogel viscosity while slowly increasing the stress the hydrogel is exposed to (Figure 3a,c). At stresses below

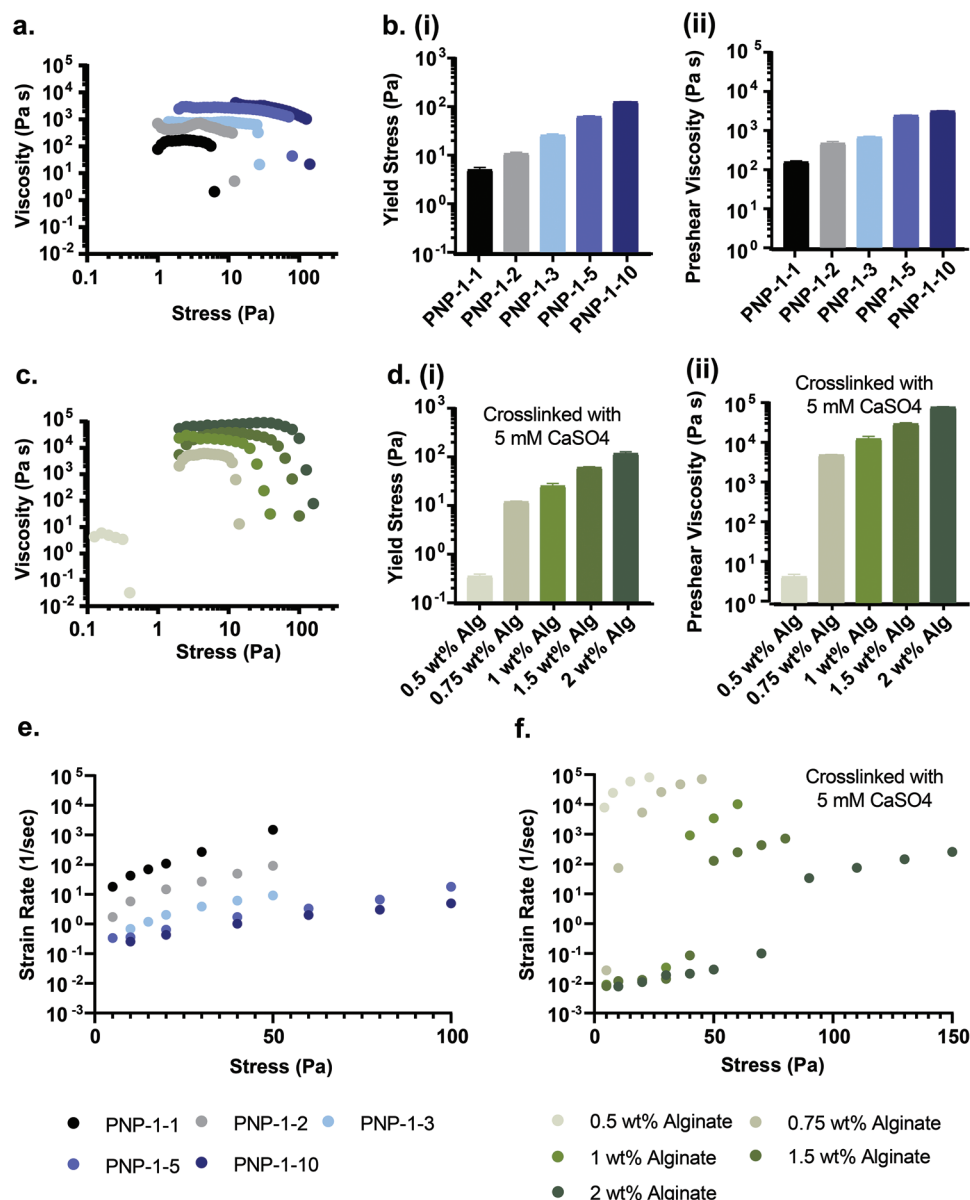


Figure 3. PNP and Alginate hydrogels exhibit tunable yield stress, preshear viscosity, and creep behavior. a). Stress-controlled yield stress measurement of PNP hydrogels. b). PNP hydrogel i) yield stress and ii) pre-shear viscosity. c). Stress-controlled yield stress measurement of calcium-alginate hydrogels. d). Calcium-alginate hydrogel i) yield stress and ii) pre-shear viscosity. e). Creep performance of PNP hydrogels. f). Creep performance of calcium-alginate hydrogels. Values reported in plots b and d are mean \pm SD of $n = 3$.

the hydrogel's yield stress, the material does not flow and exhibited a high preshear viscosity. When the stress exceeds the hydrogel's yield stress, the material starts to flow, and the viscosity was observed to drop significantly. As NP content of PNP hydrogels increases, the cross-link density increases and resulted in an increase in both the material's yield stress and preshear viscosity prior to yielding (Figure 3b).

Calcium-alginate hydrogels exhibited similar rheological trends as alginate polymer content is increased. We created five distinct calcium-alginate hydrogels with a uniform calcium sulfate concentration of 5 m_m and varied alginate weight percent of 0.5, 0.75, 1, 1.5 and 2 wt.% alginate. As alginate content increased, these hydrogels showed increased yield stress and increased preshear viscosity prior to yielding (Figure 3d). It is interesting to note that while PNP hydrogels and alginate hydrogels exhibited nearly matched yield stresses, calcium-alginate hydrogels showed much higher preshear viscosities.

Creep is an additional rheological property that we hypothesized to be relevant to depot persistence time following subcutaneous administration. A creep test studies the deformation of a material following exposure to a small but constant stress (Figures S3 and S4, Supporting Information). PNP hydrogel formulations exhibited lower strain rates at a given stress with increased NP content, and the observed strain rate within a given formulation increases log-linearly with stress (Figure 3e). Calcium-alginate hydrogels exhibited distinct creep behavior, whereby strain rate below the yield stress was small, but exhibited a significant increase above the yield stress. Moreover, the strain rate observed above the yield stress is lower for stiffer materials comprising higher alginate content (Figure 3f). The unique creep behavior of the PNP and alginate hydrogels likely arises from large differences in the rates of association and disassociation of the physical crosslinks in these systems. PNP hydrogels have highly dynamic crosslinks that break and reform rapidly even when the hydrogels are exposed to stresses exceeding its yield stress. Calcium-alginate hydrogels behave more similarly to covalently crosslinked materials, whereby the crosslinks remain intact below the yield stress when the material is not flowing, but break apart above the yield stress, resulting in a rapidly straining material unable to recover its network structure.

2.2. Depot Formation and Persistence Following Injection in the Subcutaneous Space

We hypothesized that hydrogel depot formation and persistence following subcutaneous administration can be predicted by hydrogel rheology. Specifically, we expected yield stress to be predictive of depot formation and creep behavior to be predictive of depot persistence. To probe this question, we subcutaneously injected fluorescently tagged calcium-alginate and PNP hydrogel formulations (100 μL) exhibiting variable mechanical behaviors across a range of rheological properties (stiffness, tan delta, yield stress, and creep). We then utilized brightfield photographic images collected with a standard camera and fluorescent images collected from an *in vivo* Imaging System (IVIS) to study depot formation and persistence at the site of injection. Additional rheological characterization was performed to ensure

materials properties measured at 25 °C are comparable to those measured at *in vivo* temperatures of 37 °C (Figures S5 and S6, Supporting Information).

2.2.1. The Role of Hydrogel Yield Stress in Predicting Depot Formation

If the yield stress of the hydrogel is less than the stresses exerted by the tissue in the subcutaneous space, we would expect the hydrogel to flow and flatten. In contrast, if the yield stress of the hydrogel is greater than these stresses, we would expect the hydrogel to maintain its shape and form a robust, roughly spherical depot. We observed with both PNP (Figure 4a) and calcium-alginate (Figure 5a) hydrogels that there exists a minimum hydrogel yield stress needed to prevent immediate flattening after administration in the subcutaneous space. Hydrogels with yield stresses ≤12 Pa flatten shortly after administration while hydrogels with yield stresses ≥25 Pa persist as stable depots for more than two weeks. From these observations, we estimate the stress of the subcutaneous space of a mouse to be between 12 and 25 Pa. Additionally, although the depots of low yield stress hydrogels appear to flatten shortly after administration, it is evident from fluorescent IVIS imaging of the injection site that the hydrogel components are still present at the site of injection two weeks later, though with poorly defined shape (Figures 4b and 5b).

2.2.2. Quantification of Depot Persistence

For both PNP and calcium-alginate hydrogels, formulation dramatically impacts depot persistence time whereby stiffer hydrogel formulations persist for a longer time (Figure 6a). PNP-1-1, PNP-1-2, PNP-1-3, PNP-1-5, and PNP-1-10 formulations persisted for 0.4, 2.9, 174, 22.6, and 24.4 days, respectively. Depot persistence time of the depot-forming PNP hydrogel formulations (e.g., PNP-1-3, PNP-1-5, PNP-1-10) was found to be statistically greater than the depot persistence time of non-depot forming formulations (e.g., PNP-1-1, PNP-1-2) with $p < 0.0001$. Following depot flattening, animals were euthanized, and no fibrotic capsule formation was observed where PNP hydrogels were injected in the subcutaneous space (Figure S7, Supporting Information).

IVIS imaging of fluorescently tagged PNP hydrogels provides further insight into gel retention in the subcutaneous space. Fluorescent signal over time from each gel injection was normalized and fit to a single-phase exponential decay curve to provide a half-life of gel retention (Figure 6b). Stiffer PNP hydrogel formulations showed increased half-lives of hydrogel retention with PNP-1-1, PNP-1-2, PNP-1-3, PNP-1-5, and PNP-1-10 formulations exhibiting average half-lives of 5.8, 5.9, 77, 8.5, and 10.9 days respectively. The increase in half-life of hydrogel retention for stiffer formulations that form more robust depots likely results from decreased rates of hydrogel erosion. However, it is clear from the similarity of fluorescent half-lives of gel retention, that gels remain present in the subcutaneous space even after flattening.

Similar trends in depot persistence are observed for calcium-alginate hydrogels, whereby stiffer calcium-alginate

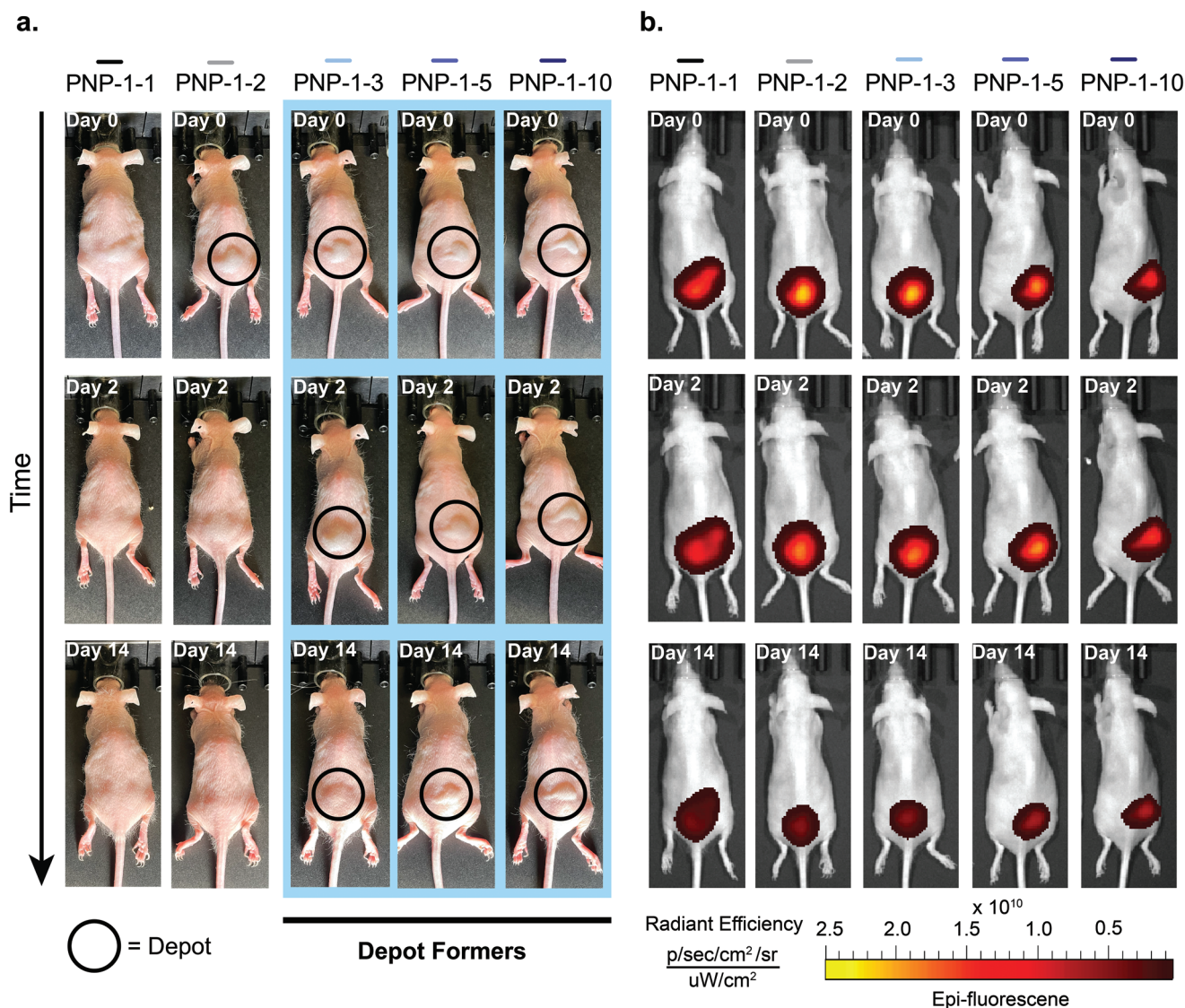


Figure 4. PNP gel rheological properties impact depot formation and persistence. a). Photographic images of PNP hydrogel depots at 0, 2, and 14 days after injection. b). IVIS images of PNP hydrogel depots at 0, 2, and 14 days after injection.

gel formulations persist for a longer time (Figure 7a). Formulations comprising 0.5 wt.% alginate, 0.75 wt.% alginate, 1 wt.% alginate, 1.5 wt.% alginate, and 2 wt.% alginate persisted for 0.3, 1.3, 26, 29, and 37 days, respectively. As one calcium-alginate hydrogel failed to flatten completely due to a deleterious immune response, we report the median hydrogel depot persistence time rather than the mean (Figure S8, Supporting Information). For all other alginate hydrogels, following depot flattening, no fibrotic capsule formation was observed where alginate hydrogels were injected in the subcutaneous space (Figure S7, Supporting Information).

Stiffer calcium-alginate hydrogel formulations again showed increased half-lives of depot retention with 0.5 wt.% alginate, 0.75 wt.% alginate, 1 wt.% alginate, 1.5 wt.% alginate, and 2 wt.% alginate formulations exhibiting average half-lives of 1.3, 1.4, 1.7, 1.9, and 3.1 days, respectively (Figure 7b). The shorter half-life fit for calcium-alginate hydrogels as compared to PNP

hydrogels likely results from calcium-alginate gels having a steeper initial fluorescence decay followed by a more gradual fluorescence decay at later timepoints (Figure 7b(i)). At 3 weeks, PNP hydrogels exhibited an average normalized fluorescence of 0.16 as compared to calcium-alginate hydrogels, which exhibited an average normalized fluorescence of 0.27. While the half-life of fluorescence decay for calcium-alginate hydrogels may be influenced by an early loss of fluorescence, overall fluorescence retention is longer for calcium-alginate hydrogels as compared to PNP hydrogels, corroborating the observed increase in depot persistence time.

2.2.3. Materials Properties Contributing to Extended Depot Persistence

To identify rheological properties that are predictive of depot persistence time, we plotted hydrogel storage modulus, tan

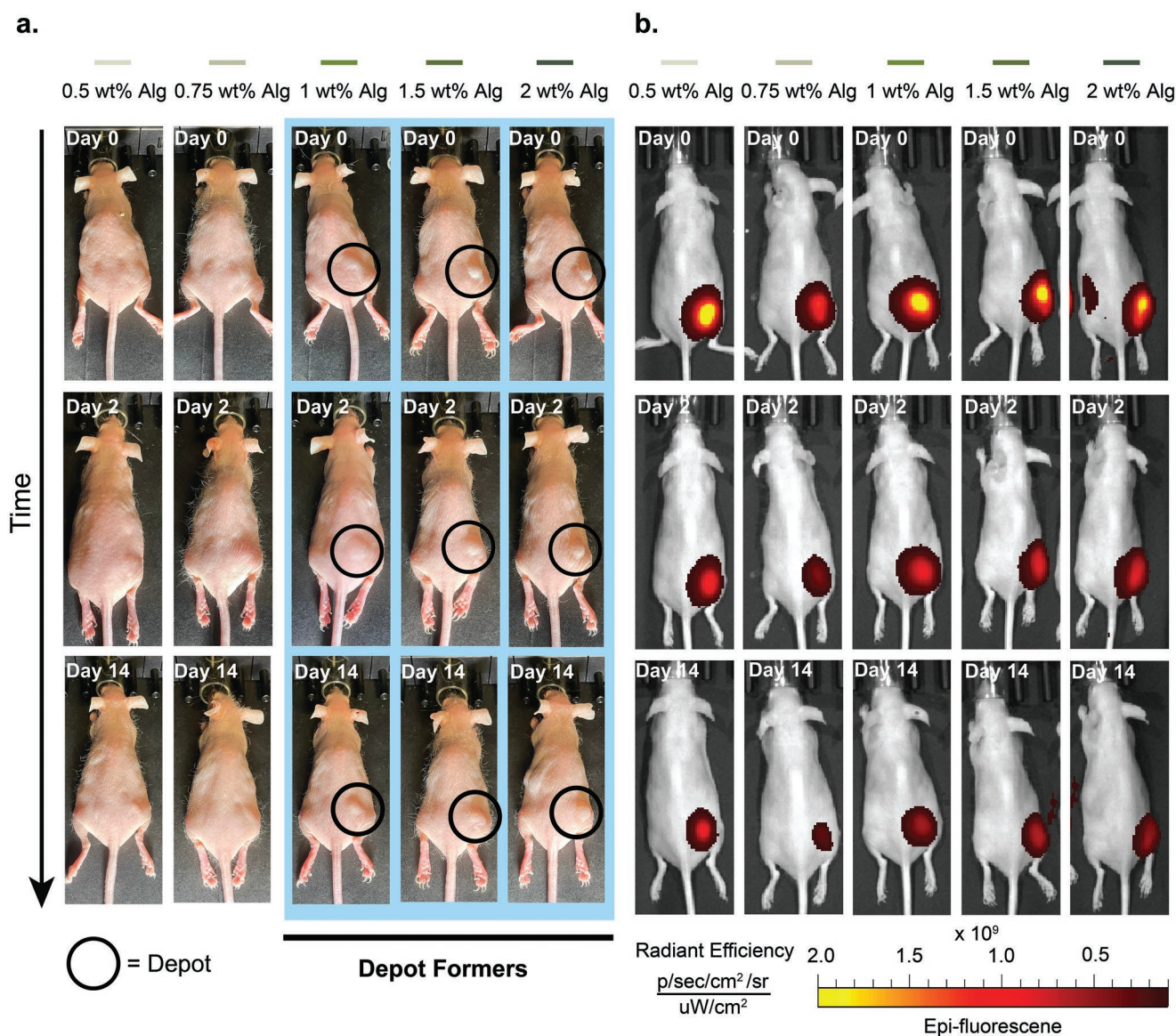


Figure 5. Alginate gel rheological properties impact depot formation and persistence. a). Photographic images of calcium-alginate hydrogel depots at 0, 2, and 14 days after injection. b). IVIS images of calcium-alginate hydrogel depots at 0, 2, and 14 days after injection.

delta, yield stress, and preshear viscosity against the depot persistence time for each hydrogel formulation (Figure 8). Although no single property fully predicts depot persistence time, it was apparent that persistence time of both hydrogel types increased with increasing storage modulus, yield stress, and preshear viscosity. Tan delta, a measure of relative elasticity of the hydrogels, does not appear to be universally predictive of depot persistence time. Indeed, PNP hydrogels showed a decrease in depot persistence time with increasing tan delta while calcium-alginate hydrogels showed an increase in depot persistence time with increasing tan delta.

While storage modulus, yield stress, and preshear viscosity are somewhat predictive of depot persistence time, they fail to explain the significantly higher depot persistence times of yield stress matched calcium-alginate hydrogels as compared to PNP hydrogels. One important way these hydrogel classes vary in

their mechanical behavior is in their creep performance. We showed that the strain rates the hydrogels experience at a stress relevant to the subcutaneous space (e.g. 12–25 Pa) is highly predictive of relative depot persistence time. Indeed, the relative strain rates the hydrogels experience at a stress of 12–25 Pa is indicative of depot persistence time for both depot-forming and non-depot-forming, yield-stress-matched PNP and calcium-alginate hydrogels.

For non-depot-forming hydrogels with a yield stress of 12 Pa, calcium-alginate gels exhibit a significantly higher strain rate than PNP hydrogels at a stress relevant to the subcutaneous space. These calcium-alginate materials, experiencing more strain at the relevant stress, exhibit a decrease in depot persistence time compared to their PNP hydrogel counterparts (Figure 9a). In contrast, for depot-forming hydrogels with yield stresses of 25, 60, and 120 Pa, calcium-alginate gels exhibit a

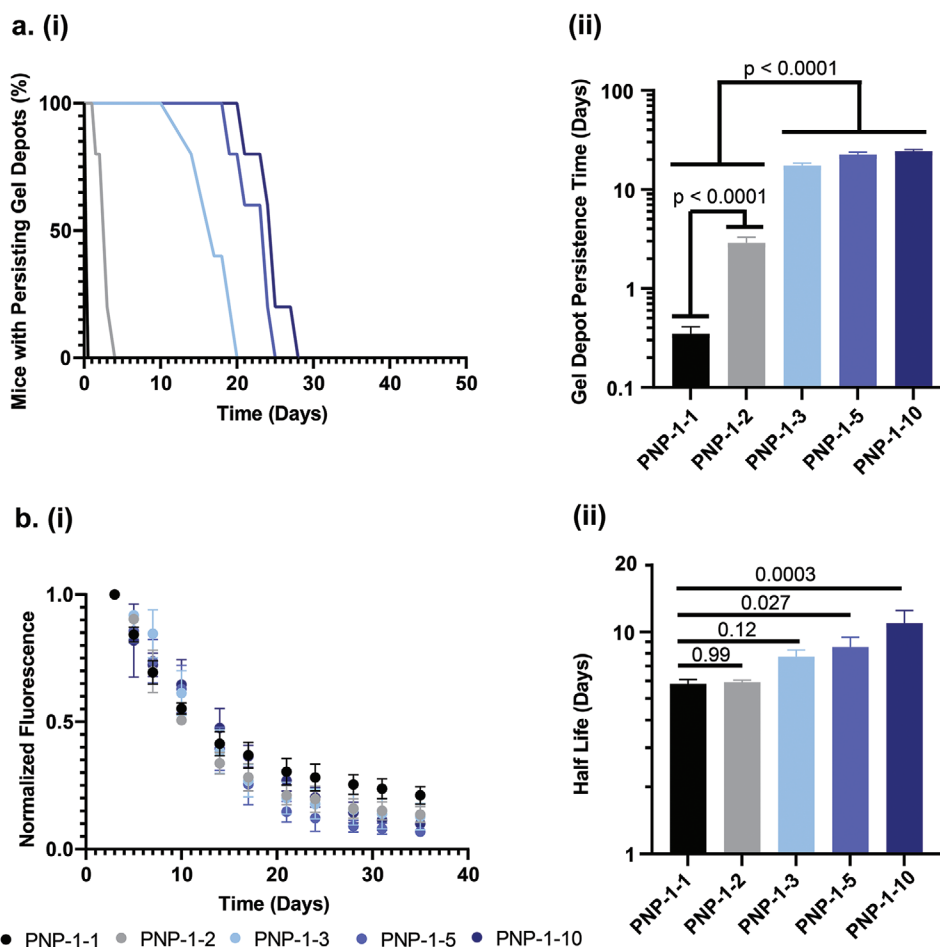


Figure 6. Increasing nanoparticle content in PNP hydrogels increases depot persistence time and half-life of gel retention in the subcutaneous space. a). i) Fraction of mice with persisting gel depots over time from each PNP formulation and ii) average depot persistence time for each PNP formulation. b). i) Curves illustrating average fluorescent signal decay from PNP gels and ii) half-lives calculated by fitting fluorescent decay curves to a single-phase exponential decay model. Values reported are means \pm SE of $n = 5$ per group. Statistical significance values are p values obtained from a Tukey HSD test.

significantly lower strain rate than PNP gels at a stress relevant to the subcutaneous space. These calcium-alginate materials, experiencing less strain at the relevant stress, exhibit an increase in depot persistence time compared to their PNP hydrogel counterparts (Figure 9b–d).

This observation is further quantified by plotting the relationship between strain rate at a stress relevant to the subcutaneous space and depot persistence time. We observe a log-linear relationship between the strain rate observed from creep tests at 15 Pa and depot persistence time (Figure 10a). Depot-forming and non-depot-forming hydrogel formulations collapse onto separate log-linear curves, but each log-linear curve includes both physiochemically distinct hydrogel classes. These observations suggest that creep performance of physical hydrogel materials may be useful in predicting depot persistence time in vivo, which is highly relevant to numerous biomedical applications. As viscosity is a materials property frequently extracted from creep test data, we also plotted the relationship between average pre-shear viscosity obtained from stress-controlled yield stress measurements and depot persistence time (Figure 10b). As preshear viscosity is only relevant to gels forming a robust

depot, only depot-forming hydrogel formulations were included in this analysis. Again, a log-linear relationship between pre-shear viscosity and depot persistence time was observed that captured both calcium-alginate and PNP hydrogel materials, suggesting that pre-shear viscosity may have predictive power in estimating depot persistence times. Future work will be directed at confirming these trends with additional hydrogel chemistries to both assign physical meaning to the observed log-linear relationship and generate generalizable design criteria for physical hydrogel materials.

2.2.4. Additional Materials Properties Impacting Depot Persistence

This research focuses on understanding predictive rheological properties that impact depot formation and persistence in physically cross-linked hydrogel materials. PNP hydrogels and calcium-alginate hydrogels were chosen as they are physiochemically distinct, physically cross-linked hydrogel systems. When extending these findings to additional hydrogel chemistries, it will be important to consider other factors—especially

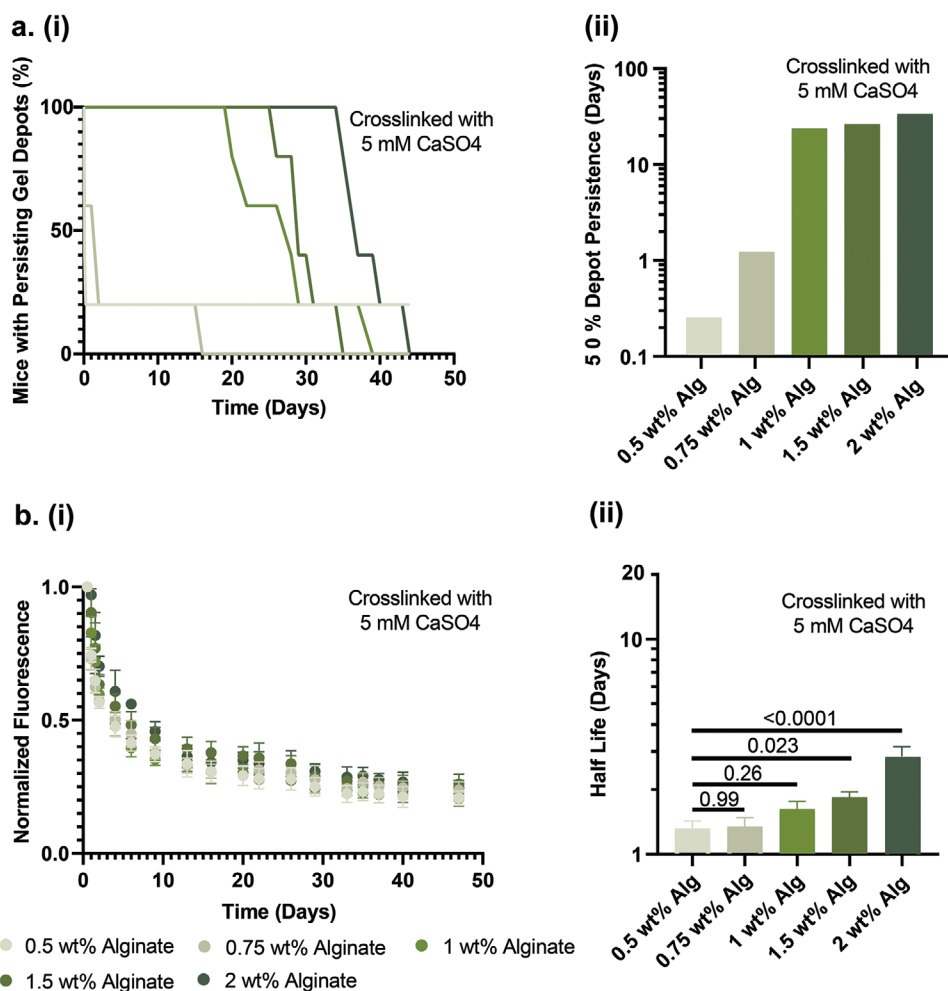


Figure 7. Increasing polymer content in alginate hydrogels increases depot persistence time and half-life of gel retention in the subcutaneous space. a). i) Fraction of mice with persisting hydrogel depots over time from each calcium-alginate formulation and ii) time when only 50% of calcium-alginate depots in each hydrogel group persist. b). i) Curves illustrating average fluorescent signal decay from calcium-alginate hydrogels and ii) half-lives calculated by fitting fluorescent decay curves to a single-phase exponential decay model. Values reported in plot *b* are means \pm SE of $n = 5$ per group. Values reported are means \pm SE of $n = 5$ per group. Statistical significance values are *p* values obtained from a Tukey HSD test.

those properties not relevant in these hydrogel materials—that may impact depot persistence time. Physically cross-linked hydrogels are unique in that they typically erode by dissolution over time and generally exhibit negligible swelling in the subcutaneous space.^[49] Significant swelling may alter hydrogel mechanical properties impacting depot persistence time as well as making identification of depot morphology more challenging. Additionally, some polymeric chemistries are more rapidly degraded and cleared by the body. For example, hyaluronic acid has a half-life in the subcutaneous space of ≈ 1 day.^[50] For these more rapidly cleared polymeric materials, creep may no longer be predictive in quantifying depot persistence time. Further, tissue adherence may impact hydrogel depot persistence; however, PNP hydrogels exhibit robust tissue adherence while alginate hydrogels do not,^[8,51] and since calcium-alginate hydrogels persist longer than PNP gels of matched yield stress we do not expect that tissue adherence contributes significantly to depot formation and persistence. Finally, it is relevant to consider the impact of an adverse immune response to the injected

material. An inflammatory response may lead to the generation of fibrotic capsules^[52] that would generally be expected to extend depot persistence, while attraction and accumulation of immune cells would generally be expected to increase the rate of hydrogel depot degradation.

2.3. Depot Formation and Persistence Enhance Control of Cargo Release Kinetics

To demonstrate that formation and persistence of a hydrogel depot of defined shape provides improved control over cargo release, we quantified the release of protein cargo from spherical and flattened hydrogel depots. PNP-1-10 hydrogels were injected into the subcutaneous space to form spherical depots, and either left as spherical depots (Figure 11b) or flattened into thin a cylindrical depot (Figure 11a). IVIS was used to image the release of fluorescently tagged bovine serum albumin (BSA) from the two geometries over 5 days (Figure 11a,b). Release

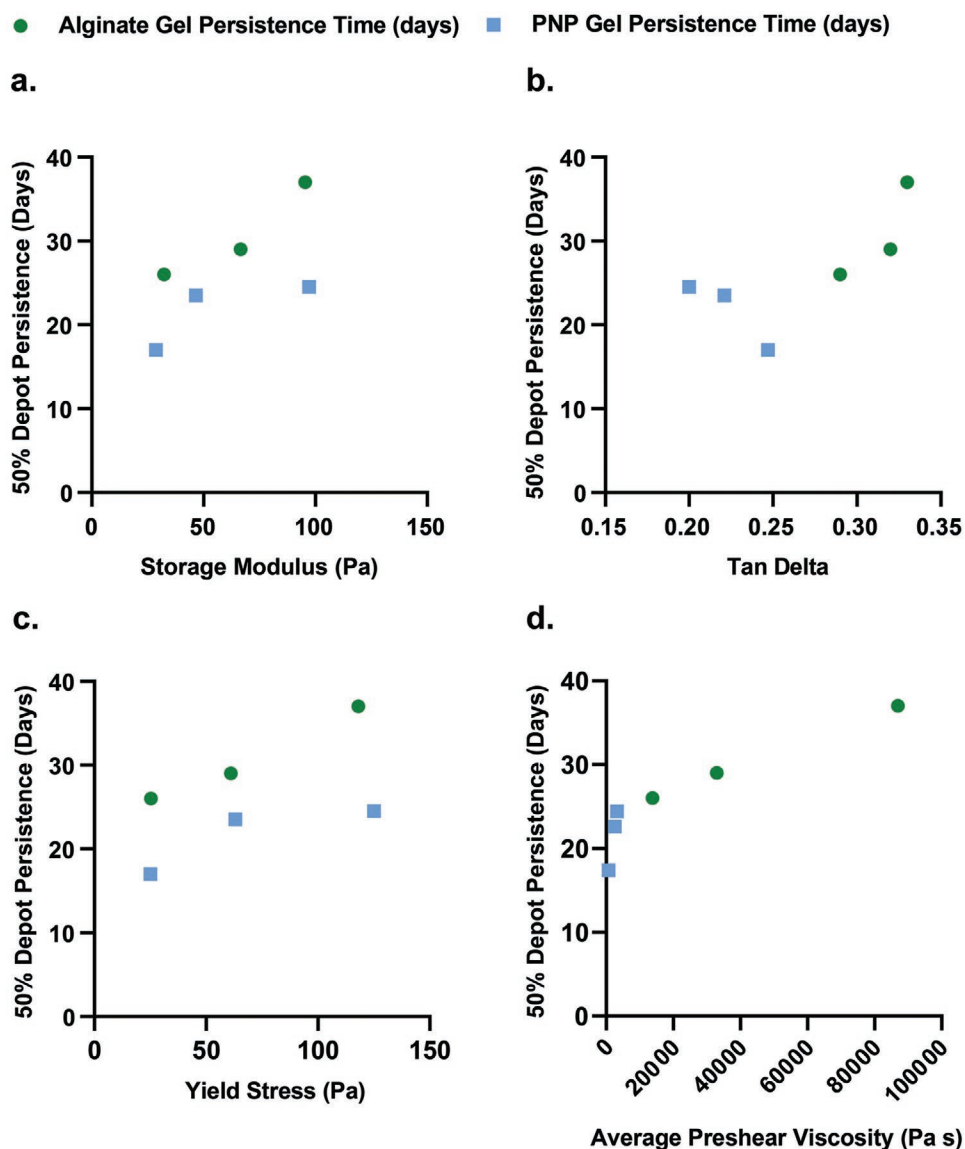


Figure 8. Storage modulus, yield stress, and viscosity are predictive of depot persistence time. Impact of a). storage modulus, b). tan delta, c). yield stress, and d). preshear viscosity on time to when only 50% of depots in each gel group persist.

from spherical hydrogel depots was slower (Figure 11c) and resulted in a twofold increase in the half-life of cargo release (Figure 11d). Measured release kinetics were comparable to those predicted from Ritger–Peppas diffusional release modeling from these geometries. For this theoretical prediction, we used dimensions for the sphere and cylinder estimated from caliper measurements and a PNP-1-10 diffusivity of $2 \text{ } \mu\text{m}^2 \text{ sec}^{-1}$ estimated from fluorescent recovery after photobleaching.^[53,54] These results further highlight the importance of depot formation and persistence to enhance control of cargo release.

3. Conclusion

Understanding how hydrogel properties affect depot formation following administration in the body is crucial to the development

of controlled release technologies. In this work, we evaluated how hydrogel rheology can be used to predict depot formation and persistence following subcutaneous administration in mice. We utilized both calcium-alginate hydrogels and PNP hydrogels, which are two physiochemically distinct, physically cross-linked hydrogel systems. These hydrogel systems are formulated to exhibit variable mechanical behaviors across a range of important rheological properties (stiffness, tan delta, yield stress, and creep), and the added advantage of calcium-alginate and PNP hydrogels with matched yield stresses allowed for the decoupling of the impacts of yield stress and creep behaviors. By relating measured rheological properties to depot persistence time when injected into the subcutaneous space of mice, we identify that for these two gel systems yield stress is predictive of initial depot formation while creep is predictive of depot persistence. Hydrogels with yield stresses $>25 \text{ Pa}$ form robust depots, and depot

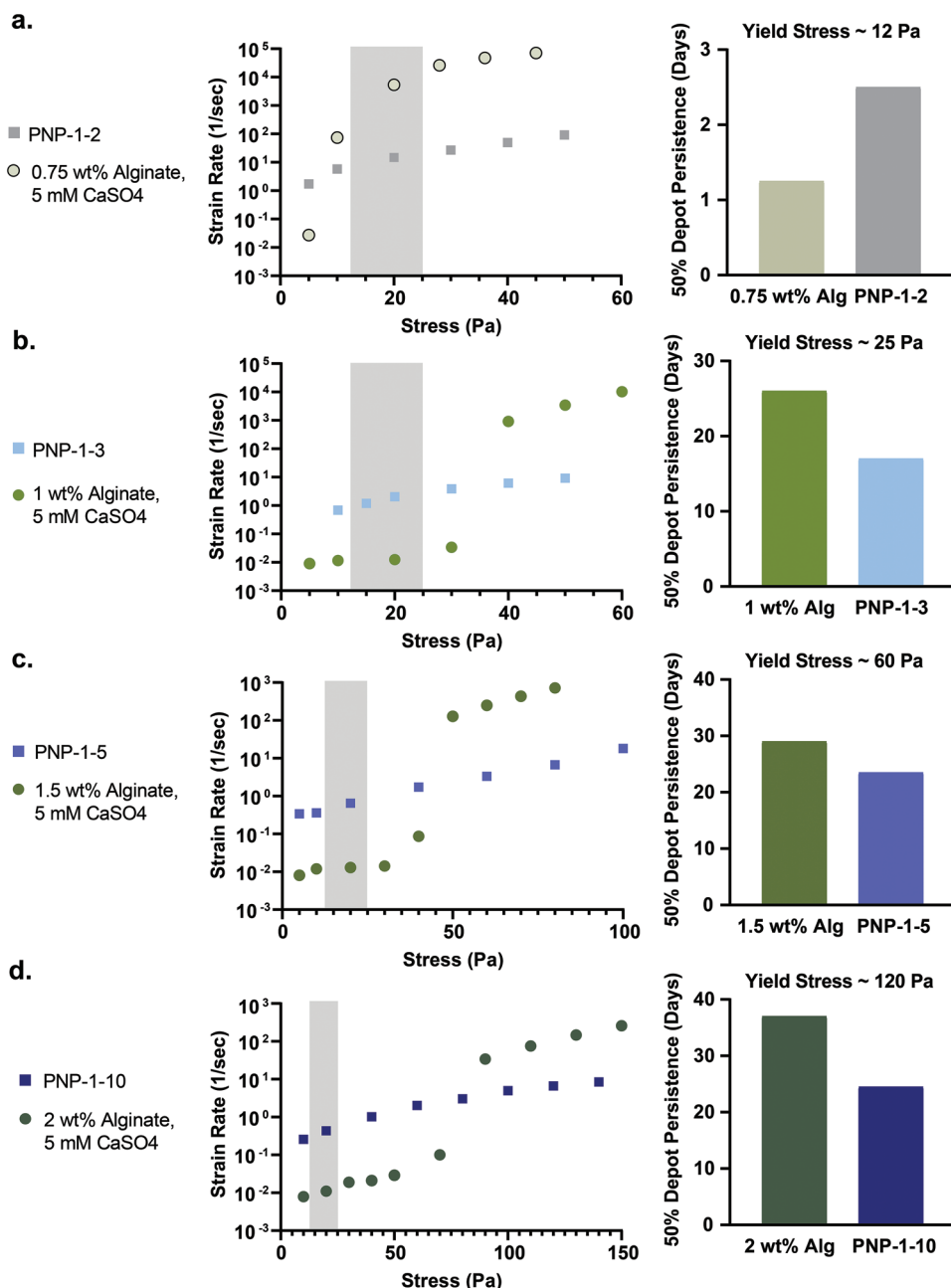


Figure 9. Relative strain rate at a stress relevant to that experienced in the subcutaneous space is predictive of depot persistence time. Graphs illustrating relationship between strain rate and applied stress as well as depot persistence time for yield-stress matched PNP and alginate hydrogels with yield stresses of a). 12 Pa, b). 25 Pa, c). 60 Pa, and d). 120 Pa.

persistence time is log-linearly related to the strain rate values obtained from creep tests. These findings provide predictive insights into design considerations for hydrogel technologies capable of extended controlled release of therapeutic cargo.

4. Experimental Section

Materials: Sodium alginate was purchased from Bioworld (CAS:9005-38-3, Mn ≈210 kDa). Racemic lactide (3,6-dimethyl-1,4-dioxane-2,5-dione, 99%, Sigma–Aldrich) was twice recrystallized from dry ethyl acetate to

remove impurities. Prior to the first recrystallization, sodium sulfate was included as a desiccant. Before use, dichloromethane (DCM) was dried by cryogenic distillation. Monomethoxy-PEG and monomethoxy-PEG-azide (5 kDa) were purchased from Sigma–Aldrich. Prior to use, monomethoxy-PEG and monomethoxy-PEG-azide were purified by azeotropic distillation with toluene. AF647-DBCO was purchased from Thermo Fisher and used as received. Sulfo-Cyanine7 amine was purchased from Lumiprobe and used as received. HPMC (USP grade), *N,N*-Diisopropylethylamine (Hunig's base), diethylether, hexanes, *N*-methyl-2-pyrrolidone (NMP), 1-dodecylisocyanate, diazobicycloundecene (DBU), 2-(*N*-morpholino) ethanesulfonic acid (MES), 1-Ethyl-3-(3 dimethylaminopropyl) carbodiimide (EDC),

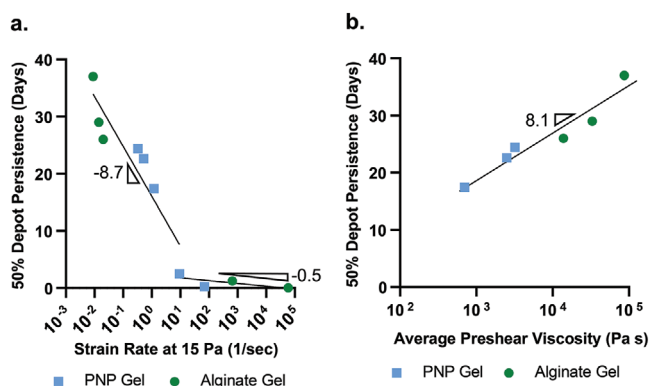


Figure 10. Strain rate and preshear viscosity are predictive of depot persistence time. a). Log-linear relationship between strain rate at 15 Pa and time when only 50% of depots in each gel group persist. b). Log-linear relationship between preshear viscosity and time when only 50% of depots in each gel group persist.

N-hydroxysulfosuccinimide (NHS) sulfo ester, and all other materials were purchased from Sigma–Aldrich and used as received.

Poly(ethylene)-block-poly(lactic acid) Synthesis: Poly(ethylene glycol)-block-poly(lactic acid) (PEG-PLA) block copolymers were synthesized using a ring opening polymerization method described in prior work.^[38] The resultant product's molecular weight and dispersity were characterized by DMF SEC (22.5–27.5 kDa (5 kDa PEG, 17.5–22.5 kDa PLA) with $\bar{D} < 1.2$).

PEG-PLA Nanoparticle Synthesis: Core-shell PEG-PLA nanoparticles were synthesized using a nanoprecipitation method described in prior work.^[38] Briefly, PEG-PLA (50 mg) was dissolved in a solution of 75:25 acetonitrile:DMSO (1 mL). The dissolved polymer was added dropwise to ultrapure water (10 mL) stirred at a high stir rate (600 rpm). The resultant nanoparticle solution was concentrated through centrifugation using a filter (Amicon Ultra-15, threshold molecular weight 10 kDa), and nanoparticles were resuspended at 20 wt.% in PBS. Dynamic light scattering (DLS, DynaPro II plate reader, Wyatt Technology) was used to characterize nanoparticle hydrodynamic diameter (30–35 nm; PDI < 0.2).

Fluorescent PEG-*b*-PLA Nanoparticle Synthesis: PEG-PLA nanoparticles were fluorescently tagged with an alexa fluor 647 dye according to procedures described in prior work.^[54] In brief, nanoparticles were synthesized using a combination of PEG-PLA and azide-PEG-PLA. Nanoparticles were conjugated with dye by mixing AF647-DBCO (25 μ L, 1 mg mL⁻¹) with azide-functional nanoparticles (250 μ L, 20 wt.%) and waiting 12 h.

Dodecyl-Modified (hydroxypropyl)methylcellulose (HPMC-C₁₂) Synthesis: Dodecyl-modified (hydroxypropyl)methyl cellulose (HPMC) was synthesized using previously described methods.^[38] The final HPMC-C₁₂ product was lyophilized and redissolved in phosphate buffered saline (PBS) as a 6 wt.% stock solution. A representative H-NMR analysis of both starting materials (Hypromellose (USP grade, 1 g) and dodecyl isocyanate (99%, 125 μ L, 0.52 mmol)) and HPMC-C₁₂ was published.^[34,54] H-NMR analysis indicated an 8.5 wt.% dodecyl modification compared to theoretical max of 10 wt.% modification of HPMC-C₁₂.^[54]

Polymer-Nanoparticle Hydrogel Synthesis: Supramolecular PNP hydrogels were formulated according to methodology described in prior work.^[36,38] In brief, HPMC-C₁₂ stock solutions and PEG-PLA nanoparticle stock solutions were combined with PBS at the desired concentrations via elbow mixing. Formulation notation for PNP hydrogels was HPMC-C₁₂ wt.% – NP wt.%. For example, a PNP-1-10 hydrogel comprises 1 wt.% HPMC-C₁₂ and 10 wt.% NPs (i.e., 11 wt.% total solids), with the remainder of the hydrogel comprised of PBS. To create a PNP-1-10 hydrogel, a HPMC-C₁₂ stock solution (167 mg) was loaded into one 3 mL luer lock syringe. Nanoparticle stock solution (500 μ L) was combined with PBS (333 μ L) and loaded into a second 3 mL luer lock syringe. These syringes were connected with an elbow fitting and mixed at a fast rate for >100 cycles until a homogenous hydrogel was formed.

All other PNP hydrogel formulations (PNP-1-1, PNP-1-2, PNP-1-3, and PNP-1-5) were prepared identically using the appropriate stock solution concentrations.

Fluorescent Polymer-Nanoparticle Hydrogel Synthesis: PNP hydrogels were made according to the above procedures. Each 1000 μ L of gel contained 50 μ L of fluorescent AF647-conjugated PEG-PLA NPs and the remainder standard PEG-PLA NPs allowing for all gel formations to have matched fluorescence. For example, 1000 μ L of PNP-1-10 contained 50 μ L of fluorescent AF647-conjugated PEG-PLA NPs and 450 μ L of standard PEG-PLA NPs.

Alginate Hydrogel Synthesis: Calcium-alginate hydrogels were formulated by cross-linking sodium alginate (Bioworld CAS:9005-38-3, Mn \approx 210 kDa) with CaSO₄. Sodium alginate was dissolved in PBS at a 4 wt.% solution. CaSO₄ was added to PBS at a concentration of 250 mM to form a slurry. The 250 mM CaSO₄ slurry and the alginate stock solution were combined with PBS to form calcium-alginate hydrogels. To form a hydrogel with 5 mM CaSO₄ and 1 wt.% alginate, the CaSO₄ slurry (250 mm) was stirred rapidly and slurry solution (20 μ L) was pipetted into PBS (730 μ L) and loaded into a 3 mL luer lock syringe. Alginate stock solution (250 mg) was loaded into another 3 mL luer lock syringe. The two syringes were connected using an elbow fitting, and alginate hydrogels were mixed at a fast rate for >100 cycles until a homogenous hydrogel was formed. All other calcium-alginate hydrogel formulations (0.5, 0.75, 1.5, and 2 wt.% alginate) were prepared identically at the appropriate concentrations.

Fluorescent Tagging of Alginate: Sodium alginate (Bioworld CAS:9005-38-3) (150 mg) was dissolved in 0.1 M 2-(*N*-morpholino) ethanesulfonic acid (MES) buffer (15 mL) at a pH of 6 and stirred for 1.5 h to ensure complete dissolution. SulfoCy7 amine (2.5 mg), 1-Ethyl-3-(3-dimethylaminopropyl) carbodiimide (EDC) (72.5 mg), and *N*-hydroxysulfosuccinimide (NHS) sulfo ester (41 mg) were then added. The mixture was stirred for 20 h and transitioned from a green to dark blue color. It was then dialyzed against MilliQ water for 5 days (MWCO 3.5 kDa) and lyophilized.

Fluorescent Alginate Hydrogel Synthesis: Alginate hydrogels were made according to procedures above. Each 1000 μ L of gel contained 0.5 wt.% fluorescently tagged alginate and the remainder standard alginate allowing for all gel formations to have matched fluorescence. For example, 1000 μ L of a hydrogel comprising 5 mM CaSO₄ and 1 wt.% alginate contained 125 mg of fluorescently tagged alginate and 125 mg of standard alginate.

Rheological Characterization: Rheological testing was performed at 25 $^{\circ}$ C using a 20 mm diameter serrated parallel plate at a 500 μ m gap on a stress-controlled TA Instruments DHR-2 rheometer. Additional rheological characterization illustrates that PNP hydrogels and calcium-alginate hydrogels exhibit comparable mechanical properties at 25 and 37 $^{\circ}$ C (Figures S5 and S6, Supporting Information). Frequency sweeps were performed at a strain of 1% within the linear viscoelastic regime. Flow sweeps were performed from high to low shear rates with steady state sensing. Stress controlled yield stress measurements (stress sweeps) were performed from low to high stress with steady state sensing and 10 points per decade. Creep experiments measured strain rate at fixed stress. An initial stress of 0.5 Pa was applied to the material for 20 s. The desired stress (5–120 Pa) was then applied, and corresponding strain percent was measured for 2000 s. Strain rate at a given stress was obtained by fitting a slope for the linear region of the strain vs time curve in GraphPad Prism.

Animal Studies: Animal studies were performed with the approval of the Stanford Administrative Panel on Laboratory Animal Care (APLAC-32109) and were in accordance with National Institutes of Health guidelines.

In Vivo Imaging of PNP Gel Depots: SKH1E mice were each administered 100 μ L of PNP hydrogel into the subcutaneous tissue via transcutaneous injection. Each of the five PNP formulations had a sample size of five mice, and PNP hydrogel formulations were each cage blocked. Mice were fluorescently imaged over a series of 35 days using an in vivo Imaging System (IVIS Lago) and half-lives of gel retention were obtained from fluorescent decay data fit to a single-phase exponential decay model. Imaging procedures and data analysis methods were identical to those thoroughly described in previously published work.^[54]

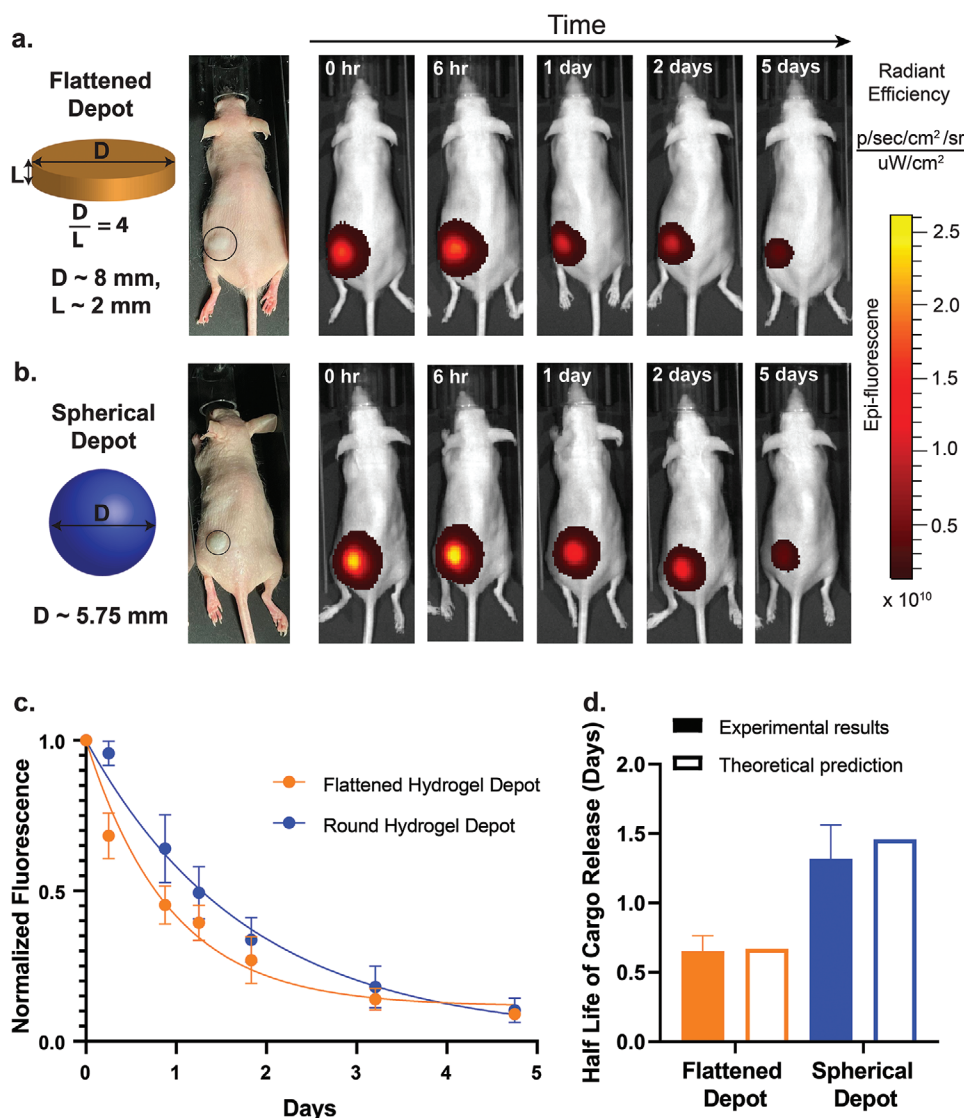


Figure 11. Hydrogel depot geometry impacts cargo release kinetics. a). Flattened depot bright field image and dimensions measured with calipers, and corresponding IVIS images of release of fluorescently tagged albumin from bovine serum (BSA). b). Spherical depot bright field image and dimensions measured with calipers, and corresponding IVIS images of release of fluorescently tagged albumin from bovine serum (BSA). c). Curves quantifying fluorescent signal decay as BSA is released from flattened and spherical hydrogel depots. d). Half-lives for cargo release calculated by fitting fluorescent decay curves to a single-phase exponential decay model. Half-lives are comparable to those predicted from Ritger-Peppas diffusional release kinetics with caliper dimensions and $D = 2 \text{ } \mu\text{m}^2 \text{ sec}^{-1}$.^[53,54] Values reported are means \pm SE of $n = 4$ per group.

In Vivo Imaging of Alginate Gel Depots: SKH1E mice were each administered 100 μL of alginate hydrogel into the subcutaneous tissue via transcutaneous injection. Each of the five alginate formulations had a sample size of five mice, and alginate hydrogel formulations were each cage blocked. Mice were imaged over 47 days using the in vivo Imaging System (IVIS Lago). Imaging procedures and data analysis were largely the same as those performed on PNP hydrogels and described in prior work.^[54] Alginate gels were imaged using an exposure time of 2 s, excitation wavelength of 720 nm, and emission wavelength of 790 nm (binning: medium, F/stop: 1.2). Total radiant efficiency was quantified and normalized to fluorescent intensity on day 0. Half-lives of hydrogel retention were obtained by fitting normalized fluorescence intensity values between day 0 and 30 to single phase exponential decay models. Data normalization and analysis was performed using GraphPad Prism.

In Vivo Imaging of BSA Release from Hydrogel Depots: SKH1E mice were each administered 100 μL of PNP-1-10 hydrogel loaded with 5 μg

of Alexa Fluor 647 conjugated albumin from bovine serum into the subcutaneous tissue via transcutaneous injection. A total of eight mice received injections. Four of the injections were kept as spherical depots and four of the injections were pressed upon to flatten immediately after injection. Dimensions of spherical and flattened depots were estimated using calipers. When imaged, mice were anesthetized with isoflurane gas. Images were collected using the in vivo Imaging System (IVIS Lago) with an exposure time of 2 s, excitation wavelength of 600 nm, and emission wavelength of 670 nm (binning: medium, F/stop: 1.2). Total radiant efficiency ($[\text{photons s}^{-1}]/[\mu\text{W cm}^{-2}]$) within an equal-sized region of interest surrounding each gel depot was quantified and normalized to total radiant efficiency on day 0. These normalized fluorescence intensity values between day 0 and day 5 for each mouse ($n = 4$) were fit to single phase exponential decay models and half-lives of cargo retention were acquired and averaged using GraphPad Prism.

Statistical Analysis: For in vivo experiments, animals were cage blocked, and Mead's Resource Equation was used to identify a sample size above that additional subjects will have little impact on power. For depot formation and persistence experiments a sample size of $n = 5$ per group was used, and no animals were considered outliers. For BSA release experiments a sample size of $n = 4$ per group was used, and no animals were considered outliers. Comparison between groups was conducted with the Tukey HSD test in JMP and values presented were means and standard errors. Results were accepted as significant if $p < 0.05$.

Supporting Information

Supporting Information is available from the Wiley Online Library or from the author.

Acknowledgements

This research was financially supported by the Center for Human Systems Immunology with the Bill & Melinda Gates Foundation (OPP1113682), the Bill & Melinda Gates Foundation (OPP1211043; INV-027411), and the American Cancer Society (RSG-18-133-01). C.K.J., J.Y., and O.M.S are thankful for National Science Foundation Graduate Research Fellowships. A.K.G. is appreciative of a National Science Foundation Graduate Research Fellowship and the Gabilan Fellowship of the Stanford Graduate Fellowship in Science and Engineering. J.B. is grateful for support from a Marie-Curie fellowship from the European Union under the program H2020, Grant 101030481.

Conflict of Interest

The authors declare no conflict of interest.

Author Contributions

C.K.J. and E.A.A. conceived of the idea. C.K.J. performed experiments. Other authors aided with experiments.

Data Availability Statement

The data that support the findings of this study are available from the corresponding author upon reasonable request.

Keywords

drug delivery, hydrogels, polymers, rheology, therapeutics

Received: March 25, 2022

Revised: July 19, 2022

Published online:

[1] In Pharmaceutical Drug Delivery Market by Route of Administration, Application, Facility of Use, COVID-19 Impact – Global Forecast to 2026, 2021.

[2] X. Y. Wang, Y. Zhang, W. Xue, H. Wang, X. Z. Qiu, Z. H. Liu, *J. Biomater. Appl.* **2017**, *31*, 923.

- [3] M. Nishikawa, K. Ogawa, Y. Umeki, K. Mohri, Y. Kawasaki, H. Watanabe, N. Takahashi, E. Kusuki, R. Takahashi, Y. Takahashi, Y. Takakura, *J. Controlled Release* **2014**, *180*, 25.
- [4] A. L. Z. Lee, V. W. L. Ng, S. J. Gao, J. L. Hedrick, Y. Y. Yang, *Biomacromolecules* **2015**, *16*, 465.
- [5] Y. Chao, Q. Chen, Z. Liu, *Adv. Funct. Mater.* **2020**, *30*, 1902785
- [6] C. Yang, N. T. Blum, J. Lin, J. L. Qu, P. Huang, *Sci. Bull.* **2020**, *65*, 1489.
- [7] M. R. Kapadia, L. W. Chow, N. D. Tsihliis, S. S. Ahanchi, J. A. Hrabie, J. Murar, J. Martinez, D. A. Popowich, Q. Jiang, J. A. Hrabie, J. E. Saavedra, L. K. Keefer, J. F. Hulvat, S. I. Stupp, M. P. Kibbe, *J. Vasc. Surg.* **2008**, *47*, 173.
- [8] L. M. Stapleton, A. N. Steele, H. Wang, H. L. Hernandez, A. C. Yu, M. J. Paulsen, A. A. A. Smith, G. A. Roth, A. D. Thakore, H. J. Lucian, K. P. Theroth, S. W. Baker, Y. Tadas, J. M. Farry, A. Eskandari, C. E. Hironaka, K. J. Jaatinen, K. M. Williams, H. Bergamasco, C. Marschel, B. Chadwick, F. Grady, M. Mae, E. A. Appel, Y. J. Woo, *Nat. Biomed. Eng.* **2019**, *3*, 611.
- [9] J. Weiden, J. Tel, C. G. Figdor, *Nat. Rev. Immunol.* **2018**, *18*, 212.
- [10] M. W. Tibbitt, K. S. Anseth, *Biotechnol. Bioeng.* **2009**, *103*, 655.
- [11] M. H. Sheridan, L. D. Shea, M. C. Peters, D. J. Mooney, *J. Controlled Release* **2000**, *64*, 91.
- [12] R. M. Thorn, J. Greenman, A. Austin, *J. Wound Care* **2006**, *15*, 305.
- [13] F. U. Momoh, J. S. Boateng, S. C. W. Richardson, B. Z. Chowdhry, J. C. Mitchell, *Int. J. Biol. Macromol.* **2015**, *81*, 137.
- [14] A. Pandit, R. Ashar, D. Feldman, *J. Invest. Surg.* **1999**, *12*, 89.
- [15] R. Jayakumar, M. Prabakaran, P. T. S. Kumar, S. V. Nair, H. Tamura, *Biotechnol. Adv.* **2011**, *29*, 322.
- [16] R. Kamel, H. A. Abbas, *Pharm. Dev. Technol.* **2013**, *18*, 990.
- [17] J. Y. Li, D. J. Mooney, *Nat. Rev. Mater.* **2016**, *1*, 1601.
- [18] N. A. Peppas, P. Bures, W. Leobandung, H. Ichikawa, *Eur. J. Pharm. Biopharm.* **2000**, *50*, 27.
- [19] B. V. Slaughter, S. S. Khurshid, O. Z. Fisher, A. Khademhosseini, N. A. Peppas, *Adv. Mater.* **2009**, *21*, 3307.
- [20] S. De Koker, R. Hoogenboom, B. G. De Geest, *Chem. Soc. Rev.* **2012**, *41*, 2867.
- [21] K. M. Cirelli, D. G. Carnathan, B. Nogal, J. T. Martin, O. L. Rodriguez, A. A. Upadhyay, C. A. Enemuo, E. H. Gebru, Y. Choe, F. Viviano, C. Nakao, M. G. Pauthner, S. Reiss, C. A. Cottrell, M. L. Smith, R. Bastidas, W. Gibson, A. N. Wolabaugh, M. B. Melo, B. Cossette, V. Kumar, N. B. Patel, T. Tokatlian, S. Menis, D. W. Kulp, D. R. Burton, B. Murrell, W. R. Schief, S. E. Bosinger, A. B. Ward, et al., *Cell* **2019**, *177*, 1153.
- [22] G. A. Roth, V. C. T. M. Picece, B. Ou, W. Luo, B. Pulendran, E. A. Appel, *Nat. Rev. Mater.* **2022**, *7*, 174.
- [23] S. Correa, A. K. Grosskopf, H. L. Hernandez, D. Chan, A. C. Yu, L. M. Stapleton, E. A. Appel, *Chem. Rev.* **2021**, *121*, 11385.
- [24] H. L. Hernandez, J. W. Souza, E. A. Appel, *Macromol. Biosci.* **2021**, *21*, 2000295.
- [25] J. L. Mann, A. C. Yu, G. Agmon, E. A. Appel, *Biomater. Sci-Uk* **2017**, *6*, 10.
- [26] M. J. Webber, E. A. Appel, E. W. Meijer, R. Langer, *Nat. Mater.* **2016**, *15*, 13.
- [27] H. Kim, H. Park, S. J. Lee, *Sci. Rep-Uk* **2017**, *7*, 6654.
- [28] C. W. Tornøe, H. Agero, H. A. Nielsen, H. Madsen, E. N. Jonsson, *Pharm. Res-Dordr* **2004**, *21*, 574.
- [29] J. P. R. Jockel, P. Leuenberger, O. Shergold, *J. Diabetes Sci. Technol.* **2013**, *7*, 227.
- [30] N. W. Kang, S. Y. Yoon, S. Kim, N. Y. Yu, J. H. Park, J. Y. Lee, H. J. Cho, D. D. Kim, *Pharmaceutics* **2021**, *13*, 864.
- [31] P. L. P. Ritger, N. A. J. *Controlled Release* **1987**, *5*, 23.
- [32] A. C. Yu, H. D. Lian, X. Kong, H. L. Hernandez, J. Qin, E. A. Appel, *Nat. Commun.* **2021**, *12*, 746.
- [33] E. A. Appel, M. W. Tibbitt, M. J. Webber, B. A. Mattix, O. Veishe, R. Langer, *Nat. Commun.* **2015**, *6*, 6295.

- [34] A. C. Yu, A. A. A. Smith, E. A. Appel, *Mol. Syst. Des. Eng.* **2020**, *5*, 401.
- [35] G. A. Roth, E. C. Gale, M. Alcantara-Hernandez, W. Luo, E. Axpe, R. Verma, Q. Yin, A. C. Yu, H. L. Hernandez, C. L. Maikawa, A. A. A. Smith, M. M. Davis, B. Pulendran, J. Idoyaga, E. A. Appel, *ACS Central Sci.* **2020**, *6*, 1800.
- [36] A. K. Grosskopf, G. A. Roth, A. A. A. Smith, E. C. Gale, H. L. Hernandez, E. A. Appel, *Bioeng. Transl. Med.* **2020**, *5*, e10147.
- [37] A. C. Yu, H. L. Hernandez, A. H. Kim, L. M. Stapleton, R. J. Brand, E. T. Mellor, C. P. Bauer, G. D. McCurdy, A. J. Wolff, D. Chan, C. S. Criddle, J. D. Acosta, E. A. Appel, *P. Natl. Acad. Sci. USA* **2019**, *116*, 20820.
- [38] C. M. Meis, E. E. Salzman, C. L. Maikawa, A. A. A. Smith, J. L. Mann, A. K. Grosskopf, E. A. Appel, *ACS Biomater. Sci. Eng.* **2021**, *7*, 4221.
- [39] F. Abasalzadeh, S. V. Moghaddam, E. Alizadeh, E. Akbari, E. Kashani, S. M. B. Fazljou, M. Torbati, A. Akbarzadeh, *J. Biol. Eng.* **2020**, *14*, 8.
- [40] K. Y. Lee, D. J. Mooney, *Prog. Polym. Sci.* **2012**, *37*, 106.
- [41] M. Yin, F. Xu, H. F. Ding, F. Tan, F. F. Song, J. W. Wang, *J. Tissue Eng. Regener. Med.* **2015**, *9*, 1088.
- [42] Y. Shtenberg, M. Goldfeder, H. Prinz, J. Shainsky, Y. Ghantous, I. Abu El-Naaj, A. Schroeder, H. Bianco-Peled, *Int. J. Biol. Macromol.* **2018**, *111*, 62.
- [43] D. M. Hariyadi, N. Islam, *Adv. Pharm. Pharm. Sci.* **2020**, *2020*, 8886095.
- [44] F. E. Freeman, D. J. Kelly, *Sci. Rep-Uk* **2017**, *7*, 17042.
- [45] A. K. Grosskopf, O. A. Saouaf, H. L. Hernandez, E. A. Appel, *J. Polym. Sci.* **2021**, *59*, 2854.
- [46] H. J. Kong, K. Y. Lee, D. J. Mooney, *Polymer* **2002**, *43*, 23.
- [47] K. Y. Lee, D. J. Mooney, *Prog. Polym. Sci.* **2012**, *37*, 106.
- [48] H. P. Lee, L. Gu, D. J. Mooney, M. E. Levenston, O. Chaudhuri, *Nat. Mater.* **2017**, *16*, 12.
- [49] S. W. Kim, Y. H. Bae, T. Okano, *Pharm. Res.* **1992**, *9*, 283.
- [50] E. Papakonstantinou, M. Roth, G. Karakiulakis, *Dermatoendocrinol* **2012**, *4*, 253.
- [51] L. M. Stapleton, H. J. Lucian, A. K. Grosskopf, A. A. Smith, K. P. Theroow, Y. J. Woo, E. A. Appel, *Adv. Ther.* **2021**, *4*, 2000242.
- [52] J. M. Anderson, *J. Mater. Sci. Mater. Med.* **2015**, *26*, 121.
- [53] O. M. Saouaf, G. A. Roth, B. S. Ou, A. A. A. Smith, A. C. Yu, E. C. Gale, A. K. Grosskopf, V. C. T. M. Picece, E. A. Appel, *J. Biomed. Res.* **2021**, *109*, 2173.
- [54] A. K. Grosskopf, L. Labanieh, D. D. Klysz, G. A. Roth, P. Xu, O. Adebowale, E. C. Gale, C. K. Jons, J. H. Klich, J. Yan, C. L. Maikawa, E. A. Appel, *Sci. Adv.* **2022**, *8*, 14.